Scaffold Splits Overestimate Virtual Screening Performance

Qianrong Guo¹, Saiveth Hernández-Hernández², and Pedro J. Ballester^{1*}

Department of Bioengineering, Imperial College London, London SW7 2AZ, UK
Centre de Recherche en Canc´erologie de Marseille, Marseille 13009, France
* Correspondence to: p.ballester@imperial.ac.uk

Abstract. Virtual Screening (VS) of vast compound libraries guided by Artificial Intelligence (AI) models is a highly productive approach to early drug discovery. Data splitting is crucial for the reliable benchmarking of such AI models. Traditional random data splits produce similar molecules between training and test sets, conflicting with the reality of VS libraries which mostly contain structurally distinct compounds. Scaffold split, grouping molecules by shared core structure, is widely considered to reflect this real-world scenario. However, here we show that this split also overestimates VS performance. Our study examined three representative AI models on 60 datasets from NCI-60 using scaffold split and a more realistic Uniform Manifold Approximation and Projection (UMAP)-based clustering split. We found models perform substantially worse under UMAP splits. These results highlight the need for improved benchmarks to tune, compare, and select models for VS. Our code is available at https://github.com/ScaffoldSplitsOverestimateVS/Scaffold SplitsOverestimateVS.git.

Keywords: Artificial Intelligence · Virtual Screening · Benchmarking · QSAR · Molecular Property Prediction.

1 Introduction

Virtual Screening (VS) has become a key drug discovery technique [28]. VS offers a fast and more cost-efficient method to discover novel molecules that have the potential to bind to a given target (structure-based VS) or have a specific drug response to the cell lines (phenotype-based VS). Applying the computational algorithms and models, VS can significantly reduce the time and financial burdens in the preclinical stages of drug discovery, where it accounts for over 43% of costs in the pharmaceutical industry [1]. Furthermore, VS permits screening gigascale chemical spaces [28] to guide novel drug discovery. VS can cover all the potential ranges for the drug leads, which is impossible to achieve with human labor.

^{*} Supported by CONACYT [S.H-H.] and the Wolfson Foundation and the Royal Society for a Royal Society Wolfson Fellowship [P.J.B.].

The application of Artificial Intelligence (AI) to improve VS and related problems has tremendous potential [2,25,9,10,16,23,7,40]. Many AI models achieved great performance on many benchmarks, such as the MoleculeNet [38]. However, the contribution of AI models in discovering novel molecules with potent activity is limited [22,37]. This problem might be due to the misalignment between the benchmark and the real-world challenges in drug discovery. This gap highlights the need for improving the benchmarks that more accurately represent the complexities of identifying potent new drug candidates.

Identifying the scaffold of a biologically active molecule in drug discovery is crucial. These scaffolds form the foundation for drug development through chemical modification to enhance its medicinal properties [21]. Yet, the challenge lies in the subjective nature of determining what constitutes the core scaffold and vital side chains. This challenge emphasized the need for precise methodologies in scaffold identification to contribute the new drug development.

The chemical diversity challenge is the most important roadblock to model generalization in drug discovery. Recent studies indicated the decreases in model prediction accuracy when applied to new drugs compared to new cell lines, illustrating the challenges in extrapolating across diverse chemical spaces [20,39,4,5,19].

To evaluate the model generalizability on dissimilar molecules, the scaffold split method has been proposed [38]. This splitting method splits the data into training; validation, and test sets based on the molecule scaffolds [3], offering a more challenging evaluation of model generalizability. For instance, Geometry-Enhanced molecular representation learning Method (GEM) obtained top performance on MoleculeNet against other methods using scaffold split [6].

Despite the scaffold split being praised for being realistic [36], we argue that this approach does not accurately reflect the real chemical diversity in the compound library to the models. In the vastly diverse libraries such as ZINC20 [14] and limited scaffolds represented in the training sets, scaffold split will be less representative due to the scaffolds in the training set less (even by orders of magnitude) than the scaffolds in ZINC20. While scaffold splits aim to enhance the model predictivity for dissimilar chemicals, their ability to simulate real-world situations remains debatable.

Our analysis demonstrated that the commonly used scaffold split is not realistic in that molecules with different chemical scaffolds are often similar. This has been overlooked since this split was introduced. We plan to use a split based on Uniform Manifold Approximation and Projection (UMAP) [11], which introduces more realistic distribution shifts than scaffold split. Furthermore, we argue that the ROC AUC scores used as the primary metric in MoleculeNet may not be the most effective metric for models for VS applications. The primary metric in VS is hit rate, which aims at avoiding mistaking wrong molecules as hits. Our hypothesis is that taking ROC AUC as the evaluation metric leads to many models with great performance falling short in identifying the true hit. Our study also employed a benchmark with extensive labeled data across 60 cell lines. Thereby reducing the dataset size as a limiting factor for model per-

formance evaluation in testing our hypothesis against the backdrop of chemical diversity and model generalizability.

2 Experimental design

2.1 Datasets

Our study utilized data from the US National Cancer Institute's NCI-60 cell line screening program [30], released in Oct 2020 1 . The datasets comprise data of 60 cell lines from nine tumor types: renal cancer, prostate cancer, ovarian cancer, brain cancer, colon cancer, non-small-cell lung cancer, melanoma, breast cancer, and leukemia, to help identify novel anticancer drugs. The growth inhibition conducted by a molecule on a given cell line is summarized by the GI_{50} data for all 60 cell lines. GI_{50} represents the concentration required to inhibit cell growth by 50%, serving as a key indicator of a compound's potential anticancer activity. The optimal clustering of these molecules [11] revealed seven clusters comprising 33, 118 unique molecules across all 60 cell line datasets with 1, 764, 938 GI_{50} determinations (88.8% completeness). We operate with pGI_{50} (the negative base 10 logarithm of GI_{50} in molar units). Thus, a higher pGI_{50} value corresponds to higher inhibitory potency.

2.2 Scaffold split for each of the 60 datasets

The widely used scaffold split [38] is implemented in RDKit (https://www.rdkit.org/) using the Bemis-Murcko method for scaffold identification. Compared to random splits, scaffold splits are pointed out to be more challenging for models evaluated in chemically diverse datasets [35]. To match the number of clusters used across different splitting methods, we divide the data into seven groups using scaffold splitting, such that molecules sharing the same scaffold are grouped together. This approach was performed by taking the average calculation of 33, 118 total unique molecules for seven groups, resulting in an approximate group size of 4, 731.

2.3 UMAP-based clustering split for each of the 60 datasets

We employed the UMAP-based clustering of NCI-60 molecules found optimal in a previous study [11]. In a nutshell, UMAP was employed to reduce the dimensionality of the molecular Morgan fingerprints and clustering was performed on the molecules based on their reduced dimensions. Here we define the UMAP split as taking one of these seven clusters as a test set and the rest merged for the training set. Since the number of molecules differs across clusters in UMAP splitting, we chose the cluster of 4,396 molecules as the test set for the UMAP

¹ The URL for downloading this version of NCI-60 data is: https://wiki.nci.nih.gov/display/NCIDTPdata/NCI-60+Data+Download+-+Previous+Releases.

4 Q. Guo et al.

split for single cell line comparison, which has the closest number of molecules as the test set size in the scaffold split. Lastly, for a given cell line, only the molecules with an annotated pGI_{50} for that cell line can and are retained in the corresponding data split. For each cell line, this procedure ensures that the training set and test set do not only contain different molecules, but moreover, these molecules have different chemical structures.

2.4 Comparative evaluation across the 60 datasets

To evaluate the model efficacy, we performed a seven-fold cross-validation, with 5 different seeds for each of the 60 datasets. This cross-validation employed the divided seven scaffold groups or seven molecule clusters, where each cross-validation fold used one group or cluster as a test set and the others for training.

2.5 Learning algorithms

We employed three models for comparison: the linear model Linear Regression (LR), the tree-based model Random Forest (RF), and the pre-trained graph-based deep model GEM.

LR [8] linearly models the relationships between features and pGI_{50} . The LR model was built using the Python package scikit-learn [27].

RF is a tree-based machine learning algorithm using the ensemble technique [12]. The 'Forest' refers to many simple decision trees. When building one decision tree for the RF algorithm, we first pick a subset of the same number of features as the original dataset, with the only difference being that it may include repeated data from the original dataset (bootstrapping). Then, at each training step, the random subset is used as the training set. By repeating the approach above, we will have a variety of decision trees that will form an RF model. The RF model makes the predictions by averaging the predicted pGI_{50} . This approach that applies bootstrapping and aggregation for predicting is called 'bagging'. In this study, we built the RF model for the regression task using the Python package scikit-learn [27].

Beyond the two classic machine learning baselines, we also used the pretrained regression model GEM [6], a novel approach that utilizes both molecular topology and geometry information for molecular representation learning. GEM adapts a geometry-based Graph Neural Network (GeoGNN) model pre-trained on 20 million unlabeled molecules from ZINC15 [32], which considers atoms, bonds, and bond angles in a molecule simultaneously. In our study, we loaded the pre-trained GeoGNN parameters 2 and then fine-tuned the model for our downstream pGI_{50} prediction task.

The pre-trained GeoGNN model is a graph neural network model used in GEM. It takes in an atom bond graph and a bond angle graph as inputs and

² The pre-trained parameters can be downloaded here: https://baidunlp.bj.bcebos.com/PaddleHelix/pretrained models/compound/pretrain modelschemrl gem.tgz

outputs the node representation, edge representation, and graph representation. The GeoGNN model consists of several layers of blocks, each of which contains a graph isomorphism network layer, a layer normalization layer, a graph normalization layer, a ReLU activation layer (if specified), and a dropout layer. In each of the blocks, the graph features will be updated through the aggregation process. If we assume the atom as u and (u, v) as the bonds, during the model aggregation in the graph, at the k_{th} iteration, the vectors representing the node and edge are h_u and h_{uv} . $AGGREGATE^{(k)}$ is the aggregation function in the graph neural networks, which can operate each node neighborhood before using the $COMBINE^{(k)}$ to combine all the updated node representations. The neighborhood atoms of the atom u are represented as N(u). The GeoGNN block can be formulated as (adapted from [6]):

$$a^{(k)} = AGGREGATE^{(k)} \underbrace{\{(h^{(k-1)}, h^{(k-1)}, x_{wuv}), w \in N(u)\}}_{bond-angle} \underbrace{uv \quad uw \quad uw}_{uw} \underbrace{\{(h^{(k-1)}, h^{(k-1)}, x_{wuv}), w \in N(v)\}\}}_{uv}$$
(1)

$$h_{uv}^{(k)} = COMBINE^{(k)}_{bond-angle}(h_{uv}^{(k-1)}, a_{uv}^{(k)})$$
 (2)

The GeoGNN model uses mean pooling as the readout layer to obtain the graph representation. The graph pooling layer takes in the atom bond graph, the node representation, and the edge representation as inputs and outputs the final graph representation. After the GeoGNN, it is followed by a Multilayer Perceptron (MLP), which takes the graph representation as input and predicted pGI_{50} .

To predict these *pGI*₅₀ values, two types of input features were employed:

- 1. **Molecule Descriptor Features.** A total of 263 descriptors consist of molecular Morgan fingerprints (256 bits, radius 2) and seven molecular physicochemical descriptors calculated using RDKit [17,18]. These descriptor-based features were used as input when applying the LR and RF algorithms.
- 2. **Molecular Graphs.** Molecular graphs that were constructed from the SMILES strings of the compounds were the input data for GEM [6].

2.6 Test set performance metrics

Our method for assessing model performance adopted the dual regression-classification approach, which applied a threshold of 6 on pGI_{50} values. The pGI_{50} values larger than 6 were considered as positive and below as negative. This approach allowed us to summarize predictions as True Positive (TP), True Negative (TN), False Positive (FP), and False Negative (FN), followed by evaluation metrics such as False Positive Rate (FPR) and True Positive Rate (TPR or Sensitivity) based on the prediction accuracy of the model. Metrics for VS have been explained elsewhere [33] and for convenience are summarized below.

Hit rate, our primary metric, measures the proportion of TP in compounds identified as positive, as in Equation 3, which perfectly aligns with the objective of VS: screen vast compound libraries to identify potential leads. With a high

hit rate, we are more confident in having more efficient results to find promising leads from a pool of candidates.

$$hit \ rate (\%) = \frac{TP}{TP + FN} \times 100\% \tag{3}$$

Matthews Correlation Coefficient (MCC) is a metric summarizing both types of errors:

$$MCC = \frac{TP \times TN - FP \times FN}{(TP + FP)(TP + FN)(TN + FP)(TN + FN)}$$
(4)

The Receiver Operating Characteristic (ROC) curve illustrates the performance of a binary classifier as its discrimination threshold varies. It is the plot of TPR against FPR. TPR indicates the proportion of TPs being correctly identified as such, while FPR measures the proportion of negatives being incorrectly classified as positives. Thus, the Area Under the ROC Curve (AUC) evaluates the model's ability to distinguish between the classes, which in this case are active and inactive compounds. A higher ROC AUC value indicates better model performance, with a value of 1.0 representing a perfect classifier, and a value of 0.5 indicates no discriminative power (equivalent to random guessing).

Root Mean Square Error (RMSE) is the square root of the mean of the squared differences between the actual pGI_{50} (y_i) and the model predicted pGI_{50} (y°):

$$RMSE = \frac{P_{n}(y_{i} - y^{\hat{}}_{i})^{2}}{\frac{i=1}{n}}$$
 (5)

2.7 Model hyperparameters

We used the RF implementation provided by the scikit-learn Python package [27]. The model was trained using the default settings, with the hyperparameters provided in Table 1. As for GEM, we used the pre-trained GeoGNN model parameters provided by the authors. We fine-tuned the GEM for 20 epochs on our dataset, using the default settings, including a batch size of 32, a dropout rate of 0.1, and a learning rate of 0.001. The hyperparameters used are shown in Table 2. We chose the default hyperparameters to ensure that the model could be easily compared to other models.

3 Results

3.1 Limitations of scaffold split to generate realistic VS benchmarks

The scaffold split ensures that the test set only contains molecules with new scaffolds. That is, there are no training molecules with any of these scaffolds in the test molecules. What has not been noted yet is that scaffolds are often similar and can be almost identical. Take, for instance, the 48, 416 molecules tested on the IGROV1 cell line by the NCI-60. The two most frequent scaffolds

Table 1. Hyperparameters for RF.

Hyperparameter	Default Value
n_estimators	100
criterion	squared_error
max_depth	None
min_samples_split	2
min_samples_leaf	1
min_weight_fraction leaf 0.0	
max_features	1.0
max leaf nodes	None
min impurity decrease 0.0	
bootstrap	True
max_samples	None
max_samples	None

Table 2. Hyperparameters for GEM. The head learning rate is the learning rate for the MLP after the pre-trained GeoGNN, and the encoder learning rate is the learning rate for the pre-trained GeoGNN.

Hyperparameter	Default Value
Batch Size	32
Dropout Rate	0.1
Encoder Learning Rate 0.001	
Head Learning Rate	0.001
Epoch	20

in these molecules are benzene and pyridine (Fig. 1A), which are almost identical. The scaffold split can place all benzene-containing molecules in one set and all pyridine-containing molecules in the other set. Thus, high training-test similarities are introduced by the scaffold split (Fig. 1B).

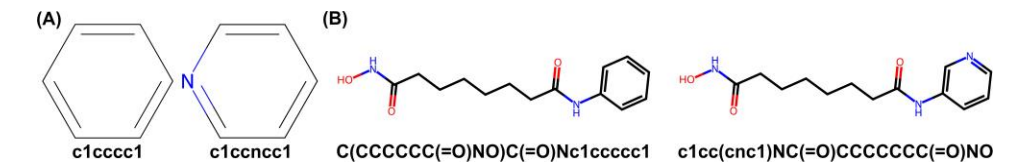


Fig. 1. Bemis-Murcko scaffolds can be almost identical, and thus the scaffold split often introduces strong training-test similarities. (A) Benzene and pyridine are the two most frequent scaffolds in the molecules tested on the NCI-60 IGROV1 cell line (each scaffold has its own SMILES string underneath). The scaffold split ensures that the test set only contains molecules with new scaffolds, i.e., no molecules in the training set have the same scaffold in the test set. (B) However, there will be molecules with similar scaffolds, which would not all be placed in the same set despite being globally similar, e.g., benzene-containing molecules could be assigned to the test set when pyridine-containing molecules are in the training set. The most similar pairs of molecules with those different scaffolds are shown. As a result, the performance of a model trained and evaluated on the scaffold split will be overestimated.

The resulting benchmarks will hence not be realistic, as the real test sets, compound libraries for prospective VS, contain not only new, but novel scaffolds [14]. Evaluating models using the scaffold split overestimates their prospective performance, as those real test sets are more complex and challenging. Thus, current benchmarks can miss the most promising models for prospective applications. There is hence an urgent need to investigate the impact of this short-

coming and provide data splits that are closer to the real level of difficulty posed by prospective VS.

3.2 GEM and RF perform similarly with scaffold split

We first started by comparing GEM to a nonlinear baseline (RF) and a linear baseline (LR). We adopted a dual regression-classification evaluation approach, wherein molecules were classified as positive and negative based on their activity cutoff at $pGI_{50} = 6$ (1 submicromolar GI_{50}). In Fig. 2, we explored the relationship between predicted and measured pGI_{50} values for molecules using scaffold split. We selected the IGROV1 cell line for this initial analysis as its results are representative of those from the other cell lines. The scaffold split was employed to train and test LR, RF, and GEM.

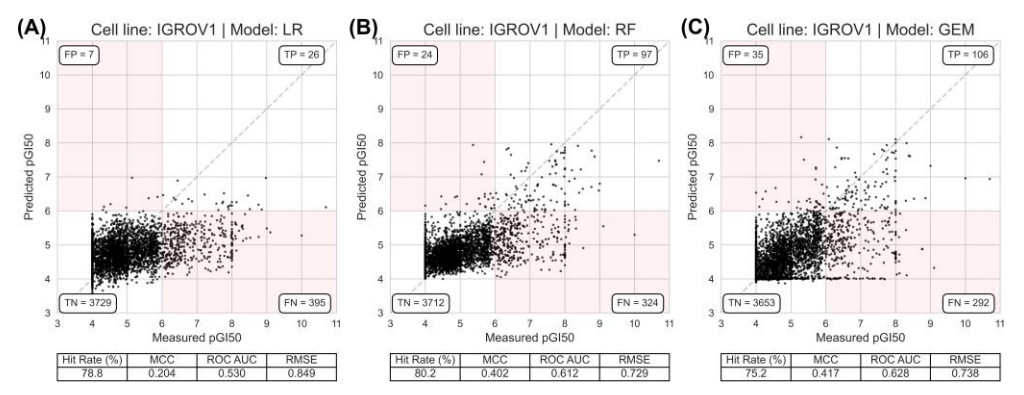


Fig. 2. Predicted pGI_{50} vs Measured pGI_{50} of molecules on the IGROV1 cell line using the scaffold split with different regression algorithms. (A) LR. (B) RF. (C) GEM. The test set contains 4, 086 on the cell line IGROV1. While constructing molecule graphs, 476 molecules from the training set and 71 molecules from the test set failed to generate the graph and were removed from the dataset for GEM.

Based on the evaluation results, RF would be the preferred model for the highest hit rate among these three models for prospective VS against the IGROV1 cell line. Even though GEM is the more complex method with the best MCC and ROC AUC scores, GEM obtained the lowest hit rate, which is the most informative metric for VS. Additionally, as GEM obtains a ROC AUC of 0.628 on IGROV1 (Fig. 2), this benchmark is much more demanding than the three using scaffold splits in MoleculeNet [38], where GEM obtains ROC AUCs of 0.806 (HIV), 0.856 (BACE), and 0.724 (BBBP) [6].

3.3 GEM outperforms RF when using the more realistic UMAP-based clustering split

Fig. 3 shows the results with the UMAP-based clustering split, which are much worse than with the overestimated scaffold split. LR and RF both exhibit a

massive drop in performance metrics, from a hit rate of about 80% to now 0%. While GEM also performed much worse on this split, it achieved a non-zero hit rate (11.9%).

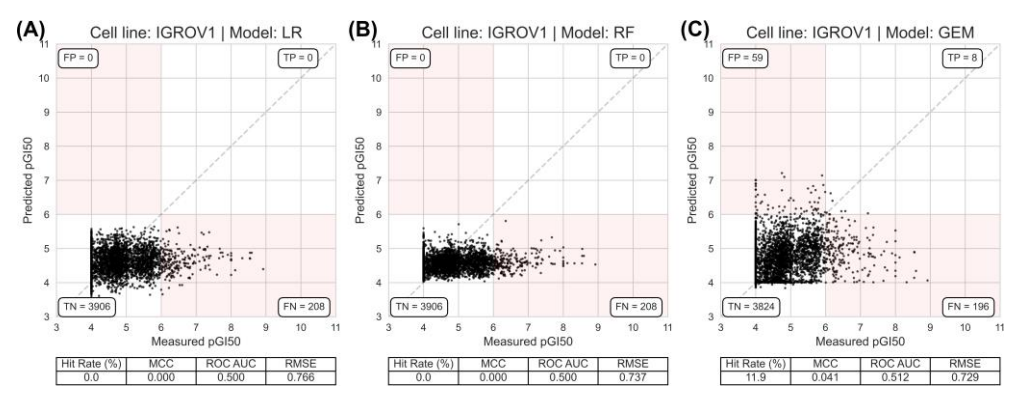


Fig. 3. Predicted pGI_{50} vs measured pGI_{50} of molecules on the IGROV1 cell line using the UMAP-based clustering split with three different regression algorithms. (A) LR. (B) RF. (C) GEM.

These results highlight the importance of selecting the right computational tool for VS. The generalizability and predictability of GEM in identifying active compounds in a challenging and realistic dataset suggest that it is better able to retrieve inhibitors with novel chemical structures for the IGROV1 cell line in prospective settings.

3.4 These results are robust across the 60 datasets

Similar trends in single cell line comparison were observed in the evaluation across all the 60 datasets as illustrated in Fig. 4. In particular, under scaffold split, RF is preferable as it has a higher median hit rate than the other two models. Despite GEM performing better in terms of the median ROC AUC score, the hit rate is deemed a more critical metric due to its importance in minimizing false positives in practical VS applications. Conversely, the UMAP split assessment, which introduces a broader and more complex testing environment, revealed that GEM outperformed RF in both the hit rate and median ROC AUC. This indicates GEM's increased efficacy in more realistic VS scenarios.

In previous paradigms when scaffold splits were widely used, the preference for scaffold splits might have led to the premature conclusion that RF was the optimal model based on the hit rate performance. However, we demonstrated that the GEM model is more adept according to UMAP split results. These results further verified our hypothesis that scaffold split overestimated the model performance and could be misleading in choosing models for practical use.

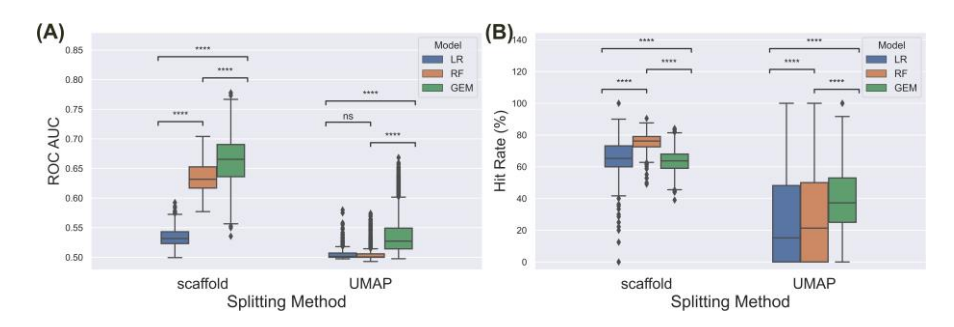


Fig. 4. Cross-validation results of the three regression algorithms across the 60 datasets, using 5 seeds and different splitting method. The performance was evaluated through two metrics: (A) ROC AUC. (B) Hit rate. P-value (p) annotation legend: ns $(5.00\times10^{-2} , *<math>(1.00\times10^{-2} , *** <math>(1.00\times10^{-3} , **** <math>(p \le 1.00\times10^{-4})$.

4 Discussion and Conclusion

The common misconception of scaffold split being able to mimic performance in real-world scenarios has been explained and demonstrated. The most ambitious objective of VS is not merely to identify active molecules with new scaffolds, but to discover those with genuinely novel scaffolds. Identifying novel scaffolds is important for discovering new therapeutic pathways and overcoming drug resistance. The scaffolds in one group are not the same as those in the other groups, but the molecules that contain them can exhibit significant similarities. In the real-world VS environment, the molecules, including their scaffolds, can be very dissimilar within the chemical space. Thus, the UMAP-based clustering split method simulates better this real-world situation. By clustering molecules based on their chemical similarity, ensuring dissimilar molecules are assigned to different sets. With the more realistic splitting method to evaluate the model's generalizability, we can be more aligned with the goal of patentable drugs with novel scaffolds.

We prioritized hit rate as the primary metric for VS, aiming to reduce false positive errors in the early drug discovery stage, which are critical for identifying potential drug leads. Furthermore, we consider MCC as the secondary metric. Unlike hit rate, MCC measures both TP and FP, without specifically valuing FP errors. Here hit rate and MCC are calculated with a cutoff, which is $pGI_{50} > 6$ as positive (hence $pGI_{50} \le 6$ as negative instance), while the most reported performances in machine learning literature are ROC AUC for classification and RMSE for regression tasks. These metrics do not align with VS goals as much as hit rate and MCC, as VS is an early recognition problem [34].

When using the scaffold split, the GEM median ROC AUC score outperforms RF across the 60 problem instances. In contrast, when using early recognition metrics, specifically hit rate, the scaffold-split median performance of GEM is

slightly worse than RF. When moving on to the UMAP-based clustering splitting method, GEM's median performances in both ROC AUC score and hit rate surpass those of RF. However, a) GEM performance was much more modest, and it declined with scaffold splitting, suggesting an overestimation, although significantly better than that of RF or LR. b) The performance of RF is indistinguishable from that of LR, with both median performances being at a random level. These findings not only referred to the potential limitations of relying on traditional methods like LR and RF for prospective VS but also highlighted the unique capabilities of deep learning models in generalization and applicability in real-world settings.

In conclusion, all the algorithms were not performing as well as they were expected. The application of the UMAP split, however, showed the true efficacy of the model in real-life scenarios, showing the reasons behind the limited success of AI in the drug discovery field and its ability to identify potential drugs.

Furthermore, situating our work within the broader field, specifically for the NCI-60 dataset, reveals a gap in research focused on unseen molecule prediction. Not many studies focus on unseen molecule prediction as our study but focusing on unseen cell line prediction [4]. In our study, we evaluated the model on unseen molecules, which is fundamentally different from those studies and not directly comparable to studies across different cell lines [15]. Moreover, there are a few studies in the same domain predicting drug responses using NCI-60 data, these studies primarily relied on random splits [31,24] or at most scaffold splits [26], or did not research further to make predictions [29]. Our approach, employing the UMAP-based clustering split, is a novel method in this field. This splitting method is crucial to contributing to the generalizability problem in drug discovery not just how the model performs across the biological context (i.e., on different cell lines), but also how the machine learning model can make robust and reliable drug response predictions of entirely novel chemicals.

Our study revealed the problem of scaffold split overestimating the model performance in the large NCI-60 datasets. This concern is not only present in the current NCI-60 database but also escalates in the larger data libraries. These ultra-large libraries can potentially be larger than 10²⁰ make-on-demand molecules [13]. Note that labeled molecules mostly come from in-stock libraries, the standard way to acquire them until recently [13], prior to experiments determining the label of interest (whole-cell activity in this study). Unsurprisingly, over 97% of the Bemis-Murcko scaffolds in make-on-demand libraries are unavailable from in-stock libraries [14]. This highlights that the existing models and methods may not be predictive enough for novel active compounds due to the overestimated results.

References

- 1. Austin, D., Hayford, T.: Research and Development in the Pharmaceutical Industry (2021), www.cbo.gov/publication/57025
- 2. Ballester, P.J.: The AI revolution in chemistry is not that far away (12 2023). https://doi.org/10.1038/d41586-023-03948-w

- 3. Bemis, G.W., Murcko, M.A.: The Properties of Known Drugs. 1. Molecular Frameworks. Journal of Medicinal Chemistry **39**(15), 2887–2893 (1 1996). https://doi.org/10.1021/jm9602928
- 4. Cort´es-Ciriano, I., van Westen, G.J.P., Bouvier, G., Nilges, M., Overington, J.P., Bender, A., Malliavin, T.E.: Improved large-scale prediction of growth inhibition patterns using the NCI60 cancer cell line panel. Bioinformatics (Oxford, England) 32(1), 85–95 (1 2016). https://doi.org/10.1093/bioinformatics/btv529
- 5. Ammad-ud din, M., Georgii, E., G"onen, M., Laitinen, T., Kallioniemi, O., Wennerberg, K., Poso, A., Kaski, S.: Integrative and personalized QSAR analysis in cancer by kernelized Bayesian matrix factorization. Journal of chemical information and modeling **54**(8), 2347–59 (8 2014). https://doi.org/10.1021/ci500152b
- Fang, X., Liu, L., Lei, J., He, D., Zhang, S., Zhou, J., Wang, F., Wu, H., Wang, H.: Geometry-enhanced molecular representation learning for property prediction. Nature Machine Intelligence 4(2), 1–8 (2022). https://doi.org/10.1038/s42256-021-00438-4
- 7. Fresnais, L., Ballester, P.J.: The impact of compound library size on the performance of scoring functions for structure-based virtual screening. Briefings in Bioinformatics 22(3), bbaa095 (5 2021). https://doi.org/10.1093/bib/bbaa095
- Galton, F.: Regression Towards Mediocrity in Hereditary Stature. The Journal of the Anthropological Institute of Great Britain and Ireland 15, 246–263 (2 1886). https://doi.org/10.2307/2841583
- 9. Gentile, F., Yaacoub, J.C., Gleave, J., Fernandez, M., Ton, A.T., Ban, F., Stern, A., Cherkasov, A.: Artificial intelligence–enabled virtual screening of ultra-large chemical libraries with deep docking. Nature Protocols 17(3), 672–697 (2022). https://doi.org/10.1038/s41596-021-00659-2
- Gryniukova, A., Kaiser, F., Myziuk, I., Alieksieieva, D., Leberecht, C., Heym, P.P., Tarkhanova, O.O., Moroz, Y.S., Borysko, P., Haupt, V.J.: AI-Powered Virtual Screening of Large Compound Libraries Leads to the Discovery of Novel Inhibitors of Sirtuin-1. Journal of Medicinal Chemistry 66(15), 10241–10251 (8 2023). https://doi.org/10.1021/acs.jmedchem.3c00128
- 11. Hern'andez-Hern'andez, S., Ballester, P.J.: On the Best Way to Cluster NCI-60 Molecules. Biomolecules **13**(3), 498 (2023). https://doi.org/10.3390/biom13030498
- 12. Ho, T.K.: Random decision forests. In: Proceedings of 3rd international conference on document analysis and recognition. vol. 1, pp. 278–282. Canada (1995). https://doi.org/10.1109/ICDAR.1995.598994
- 13. Hoffmann, T., Gastreich, M.: The next level in chemical space navigation: going far beyond enumerable compound libraries. Drug Discovery Today **24**(5), 1148–1156 (5 2019). https://doi.org/10.1016/J.DRUDIS.2019.02.013
- 14. J. Irwin, J., G. Tang, K., Young, J., Dandarchuluun, C., R. Wong, B., Khurelbaatar, M., S. Moroz, Y., Mayfield, J., A. Sayle, R.: ZINC20—A Free Ultralarge-Scale Chemical Database for Ligand Discovery. Journal of Chemical Information and Modeling 60(12), 6065–6073 (10 2020). https://doi.org/10.1021/acs.jcim.0c00675
- Krushkal, J., Negi, S., Yee, L.M., Evans, J.R., Grkovic, T., Palmisano, A., Fang, J., Sankaran, H., McShane, L.M., Zhao, Y., O'Keefe, B.R.: Molecular genomic features associated with in vitro response of the NCI-60 cancer cell line panel to natural products. Molecular Oncology 15(2), 381–406 (2 2021). https://doi.org/https://doi.org/10.1002/1878-0261.12849

- Kumar, N., Acharya, V.: Machine intelligence-driven framework for optimized hit selection in virtual screening. Journal of Cheminformatics 14(1), 48 (2022). https://doi.org/10.1186/s13321-022-00630-7
- 17. Landrum, G.: RDKit: Open-Source Cheminformatics Software (2016), https://github.com/rdkit/rdkit/releases/tag/Release_2016.09_4https://github.com/rdkit/rdkit/releases/tag/Release_2023_09_5
- Landrum, G., Tosco, P., Kelley, B., Ric, Cosgrove, D., sriniker, Vianello, R., gedeck, NadineSchneider, Jones, G., Kawashima, E., N, D., Dalke, A., Cole, B., Swain, M., Turk, S., Savelev, A., Vaucher, A., Wojcikowski, M., Take, I., Scalfani, V.F., Probst, D., Ujihara, K., guillaume godin, Pahl, A., Walker, R., Lehtivarjo, J., Berenger, F., strets123, jasondbiggs: rdkit/rdkit: Release 2023.09.5 (2024). https://doi.org/10.5281/zenodo.10633624
- Li, H., Peng, J., Sidorov, P., Leung, Y., Leung, K.S., Wong, M.H., Lu, G., Ballester, P.J.: Classical scoring functions for docking are unable to exploit large volumes of structural and interaction data. Bioinformatics 35(20), 3989–3995 (10 2019). https://doi.org/10.1093/bioinformatics/btz183
- Li, M., Wang, Y., Zheng, R., Shi, X., Li, Y., Wu, F.X., Wang, J.: DeepDSC: A Deep Learning Method to Predict Drug Sensitivity of Cancer Cell Lines. IEEE/ACM Transactions on Computational Biology and Bioinformatics 18(2), 575–582 (3 2021). https://doi.org/10.1109/TCBB.2019.2919581
- 21. Lin, X., Liang, C., Zou, L., Yin, Y., Wang, J., Chen, D., Lan, W.: Advance of structural modification of nucleosides scaffold. European Journal of Medicinal Chemistry **214**, 113233 (2021). https://doi.org/https://doi.org/10.1016/j.ejmech.2021.113233
- Liu, G., Catacutan, D.B., Rathod, K., Swanson, K., Jin, W., Mohammed, J.C., Chiappino-Pepe, A., Syed, S.A., Fragis, M., Rachwalski, K., Magolan, J., Surette, M.G., Coombes, B.K., Jaakkola, T., Barzilay, R., Collins, J.J., Stokes, J.M.: Deep learning-guided discovery of an antibiotic targeting Acinetobacter baumannii. Nature Chemical Biology (2023). https://doi.org/10.1038/s41589-023-01349-8
- Luo, Y., Peng, J., Ma, J.: Next Decade's AI-Based Drug Development Features Tight Integration of Data and Computation. Health Data Science 2022, 9816939 (3 2024). https://doi.org/10.34133/2022/9816939
- Martorana, A., La Monica, G., Bono, A., Mannino, S., Buscemi, S., Palumbo Piccionello, A., Gentile, C., Lauria, A., Peri, D.: Antiproliferative Activity Predictor: A New Reliable In Silico Tool for Drug Response Prediction against NCI60 Panel. International Journal of Molecular Sciences 23(22), 14374 (11 2022). https://doi.org/10.3390/ijms232214374
- Mayr, A., Klambauer, G., Unterthiner, T., Steijaert, M., Wegner, J.K., Ceulemans, H., Clevert, D.A., Hochreiter, S.: Large-scale comparison of machine learning methods for drug target prediction on ChEMBL. Chemical Science 9(24), 5441–5451 (2018). https://doi.org/10.1039/C8SC00148K
- Nakano, T., Takeda, S., Brown, J.B.: Active learning effectively identifies a minimal set of maximally informative and asymptotically performant cytotoxic structure-activity patterns in NCI-60 cell lines. RSC Medicinal Chemistry 11(9), 1075–1087 (2020). https://doi.org/10.1039/D0MD00110D
- 27. Pedregosa, F., Varoquaux, G., Gramfort, A., Michel, V., Thirion, B., Grisel, O., Blondel, M., Prettenhofer, P., Weiss, R., Dubourg, V., Vanderplas, J., Passos, A., Cournapeau, D., Brucher, M., Perrot, M., Duchesnay, É.: Scikit-learn: Machine Learning in Python. Journal of Machine Learning Research 12, 2825–2830 (2011), http://jmlr.org/papers/v12/pedregosa11a.html

- Sadybekov, A.V., Katritch, V.: Computational approaches streamlining drug discovery. Nature 616(7958), 673–685 (4 2023). https://doi.org/10.1038/s41586-023-05905-z
- Shivakumar, P., Krauthammer, M.: Structural similarity assessment for drug sensitivity prediction in cancer. BMC Bioinformatics 10(9), S17 (2009). https://doi.org/10.1186/1471-2105-10-S9-S17
- 30. Shoemaker, R.H.: The NCI60 human tumour cell line anticancer drug screen. Nature reviews. Cancer **6**(10), 813–823 (10 2006). https://doi.org/10.1038/nrc1951
- 31. Singh, H., Kumar, R., Singh, S., Chaudhary, K., Gautam, A., Raghava, G.P.S.: Prediction of anticancer molecules using hybrid model developed on molecules screened against NCI-60 cancer cell lines. BMC Cancer **16**(1), 77 (2016). https://doi.org/10.1186/s12885-016-2082-y
- 32. Sterling, T., Irwin, J.J.: ZINC 15 Ligand Discovery for Everyone. Journal of Chemical Information and Modeling **55**(11), 2324–2337 (2015). https://doi.org/10.1021/acs.jcim.5b00559
- 33. Tran-Nguyen, V.K., Junaid, M., Simeon, S., Ballester, P.J.: A practical guide to machine-learning scoring for structure-based virtual screening. Nature Protocols **18**(11), 3460–3511 (2023). https://doi.org/10.1038/s41596-023-00885-w
- 34. Truchon, J.F., Bayly, C.I.: Evaluating Virtual Screening Methods: Good and Bad Metrics for the "Early Recognition" Problem. Journal of Chemical Information and Modeling 47(2), 488–508 (3 2007). https://doi.org/10.1021/ci600426e
- Vamathevan, J., Clark, D., Czodrowski, P., Dunham, I., Ferran, E., Lee, G., Li, B., Madabhushi, A., Shah, P., Spitzer, M., others: Applications of machine learning in drug discovery and development. Nature reviews Drug discovery 18(6), 463–477 (2019). https://doi.org/10.1038/s41573-019-0024-5
- 36. Wang, Y., Wang, J., Cao, Z., Barati Farimani, A.: Molecular contrastive learning of representations via graph neural networks. Nature Machine Intelligence 4(3), 279–287 (2022). https://doi.org/10.1038/s42256-022-00447-x
- 37. Wong, F., Zheng, E.J., Valeri, J.A., Donghia, N.M., Anahtar, M.N., Omori, S., Li, A., Cubillos-Ruiz, A., Krishnan, A., Jin, W., Manson, A.L., Friedrichs, J., Helbig, R., Hajian, B., Fiejtek, D.K., Wagner, F.F., Soutter, H.H., Earl, A.M., Stokes, J.M., Renner, L.D., Collins, J.J.: Discovery of a structural class of antibiotics with explainable deep learning. Nature pp. 1–9 (12 2023). https://doi.org/10.1038/s41586-023-06887-8
- 38. Wu, Z., Ramsundar, B., Feinberg, E.N.N.N., Gomes, J., Geniesse, C., Pappu, A.S., Leswing, K., Pande, V.: MoleculeNet: A Benchmark for Molecular Machine Learning. Chemical Science **9**(2), 513–530 (10 2018). https://doi.org/10.1039/C7SC02664A
- 39. Xia, F., Allen, J., Balaprakash, P., Brettin, T., Garcia-Cardona, C., Clyde, A., Cohn, J., Doroshow, J., Duan, X., Dubinkina, V., Evrard, Y., Fan, Y.J., Gans, J., He, S., Lu, P., Maslov, S., Partin, A., Shukla, M., Stahlberg, E., Wozniak, J.M., Yoo, H., Zaki, G., Zhu, Y., Stevens, R.: A cross-study analysis of drug response prediction in cancer cell lines. Briefings in Bioinformatics (9 2021). https://doi.org/10.1093/bib/bbab356
- 40. Zhang, L., Ai, H.X., Li, S.M., Qi, M.Y., Zhao, J., Zhao, Q., Liu, H.S.: Virtual screening approach to identifying influenza virus neuraminidase inhibitors using molecular docking combined with machine-learning-based scoring function. Oncotarget 8(47), 83142–83154 (2017). https://doi.org/https://doi.org/10.18632/oncotarget.20915